Discussion

We describe here a mAB, named L1, that distinguishes between virulent and attenuated CDV. We further show that the epitope recognized by this mAB is acquired after repeated passaging of virulent CDV through Vero cell cultures, and that the acquisition of this epitope coincides with loss of virulence.

Loss of virulence is a frequently-observed phenomenon after virulent viruses have been adapted to cell lines, but its mechanism is poorly understood. It appears that certain sites in the CDV genome, responsible for the loss of or the regaining of virulence are preferred sites of mutation, requiring only a very limited number of passages in an appropriate system to change in either direction [3, 15]. It is possible that such rapid changes occur on the basis of selection pressure by the host system favouring certain mutations. Considering the high mutation rate of RNA viruses [16], the alternative explanation would be the continuous presence of a number of mutants within a given virus population, with the host system favouring certain variants; loss of or return to virulence would then be a reflection of fluctuations in the numerical distribution of the different variants in the population.

It has also been proposed that adaptation can, for example, be induced by integration of host-specific cell membrane elements in the envelope of viruses replicating in a non-permissive system [3].

Virulence has been related to structural features of the viral envelope proteins [17]. Changes in the surface glycoproteins of CDV, namely of the H or F proteins, which are responsible for adhesion and fusion [18], could presumably lead to altered virulence. The reverse process, the selection of escape mutants with neutralizing mABs, to obtain attenuated virus, has been successfully performed in various viral systems [19 - 21]. However, mAB L1 binds to the NP protein of CDV. Therefore, it is possible that the observed change in the NP of CDV, coinciding with adaptation, is an epiphenomenon which is not directly responsible for the changes in pathogenicity. On the other hand, we cannot exclude the possibility that an epitope in the NP protein could influence virulence. For example, a change could lead to an altered assembly of the nucleocapsid protein, or variation in the attachment of the nucleocapsid via the matrix protein to the future envelope prior to budding of the virus from the cell membrane. Cloning and sequencing of the epitope recognized by mAB L1 will be performed in the future, and may lead to further explanation of the observed phenomena.

Acknowledgments. This work was supported by the Swiss National Science Foundation (Grant Nr. 3.956.87), the Swiss Multiple Sclerosis Society and the Wander Foundation.

1 Appel, M. J., Am. J. vet. Res. *30* (1969) 1167.
2 Bittle, J., York, Ch., and Newberne, J., Cornell Vet. *51* (1961) 359.
3 Appel, M. J., J. gen. Virol. *41* (1978) 385.
4 Fatzer, R., and Fankhauser, R., Prakt. Tierarzt *57* (1976) 280.
5 Welch, S. W., and Saif, L., Archs Virol. *101* (1988) 221.
6 Oervell, C., Sheshberadaran, H., and Norby, E., J. gen. Virol. *66* (1985) 443.
7 Zurbriggen, A., Vandevelde, M., Beranek, C. F., and Steck, A., Res. vet. Sci. *36* (1984) 270.
8 Zurbriggen, A., Vandevelde, M., Dumas, M., Griot, C., and Bollo, E., Acta neuropath. (Berlin) *74* (1987) 366.
9 Appel, M. J., and Jones, O. R., Proc. Soc. exp. Biol. Med. *126* (1967) 571.
10 Köhler, G., and Milstein, C., Nature *256* (1975) 495.
11 Dubacher, B., Thesis, University of Bern, Bern, Switzerland 1988.
12 Zurbriggen, A., Vandevelde, M., and Dumas, M., Lab. Invest. *54* (1986) 424.
13 Sternberger, L. A., in: Immunochemistry, p. 105. John Wiley and Sons, New York 1979.
14 Zurbriggen, A., Vandevelde, M., and Bollo, E., J. neurol. Sci. *79* (1987) 33.
15 Goto, H., Shen, D., and Gorham, J., Fedn Proc. *35* (1976) 1021.
16 Smith, D., and Inglis, S., J. gen. Virol. *68* (1987) 2729.
17 Rott, R., Archs Virol. *59* (1979) 285.
18 Morrison, T. G., Virus Res. *10* (1988) 113.
19 Fields, B. N., and Greene, M. I., Nature *300* (1982) 19.
20 Laver, W. G., Gerhard, W., Webster, R. G., Frankel, M. E., and Air, G. M., Proc. natl Acad. Sci. USA *76* (1979) 1425.
21 Wiktor, T. J., and Koprowski, H., J. exp. Med. *152* (1980) 99.

0014-4754/91/080842-04$1.50 + 0.20/0

The broken axis approach – a new way to analyze bi-directional circular data

B. Holmquist[a] and R. Sandberg

[a] *Dept. of Mathematical Statistics, University of Lund, S-22100 Lund, and Dept. of Ecology, University of Lund, S-22362 Lund (Sweden)*

Received 6 August 1990; accepted 20 March 1991

Abstract. A new technique is demonstrated that allows detection of bi-directional asymmetric modes in circular data. The method makes it possible to search for and find the best possible description of data sets that are distributed on a circle. It was primarily developed for analysis of avian orientation data, but it is equally well suited for circular data in general. Critical levels of statistically significant deviations from uniformity, according to analyses by the new technique, are provided.

Key words. Circular distributions; bi-directional data; asymmetrical modes; orientation; bird migration.

Orientation studies, among others, yield data points which are distributed on a circle and are analysed by using circular statistics [1]. The Rayleigh test [4] has become a universal tool for detecting the presence of one-directional (unimodal) clusters of data points that deviate from uniformity. In cases of axial data where the modes are 180° apart from each other, samples are essentially interpreted as two overlapping unimodal distributions. Such axial distributions are analyzed by transforming the bimodal samples, through doubling the angles, into unimodal angular distributions [1]. In addition to the Rayleigh test, Rao's spacing test and Watson's U_n^2 test can be used for detecting both unimodal and bimodal distributions [1], for bimodal cases by doubling the angles in the same way as when using the Rayleigh test. A common feature of all the above-mentioned tests is that the purpose, i.e. testing for unimodality or bimodality, must be specified a priori.

It is not uncommon, however, that the circular distribution at hand fails to show either a distinct one-directional mode, or two antipodally symmetric modes, but instead indicates two distinct asymmetric modes ($\approx 180°$ apart). A hypothetical example of the latter phenomenon is shown in figure 1. This pattern suggests a mixture of two unimodal distributions, the modes of which are neither coinciding, nor antipodally opposite. Such a mixture of angular distributions may occur when some individuals, but not all, in a test sample respond to a certain experimental change of external circumstances. For example, if we consider migratory birds whose orientation performance is under investigation, the angular distribution shown in figure 1 is likely to emerge if some individuals react to an experimental deflection of the horizontal geomagnetic field direction of $+90°$ (Ss_2), whereas the rest of the test sample fail to do so (Ss_1). Hence, the actual directions of the different modes are of interest, especially if one of the modes corresponds to the expected direction of 'controls', while the other mode represents the direction under experimentally manipulated circumstances.

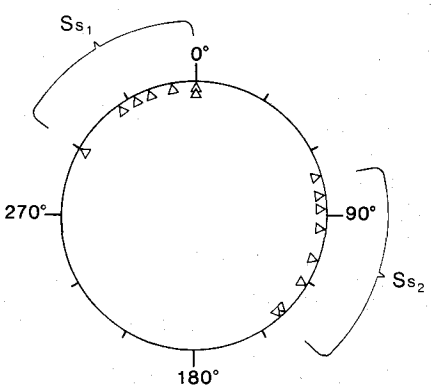

Figure 1. A hypothetical example of an asymmetric bimodal distribution. For instance, consider a sample of migratory birds tested in orientation cages, and that each triangle illustrates the directional choice of one bird. Ss_1 may then represent the proportion of individuals that fails to respond to an experimental shift of e.g., the horizontal geomagnetic field direction (magnetic north deflected $+90°$), whereas the other subsample (Ss_2) closely follow the shift. Geographic north is denoted by 0° and the rotation of angles is defined as positive (clockwise).

A new technique, the 'broken axis' approach, which allows an adequate analysis of bi-directional asymmetric circular data, will be presented in the following. It is exemplified with bird orientation data, but it should be noted that the method is equally well suited for analyzing circular data in general.

Estimating 'broken axis' modes

Current standard procedures. Let $\theta_1, \theta_2, \ldots, \theta_n$ denote the n angular directions of the data shown in figure 1. The length of the mean vector is then given by

$$r_k = \sqrt{\left(\sum_{i=1}^{n} \cos(k \cdot \theta_i)\right)^2 + \left(\sum_{i=1}^{n} \sin(k \cdot \theta_i)\right)^2}/n \qquad (1)$$

and the mean angle of the sample by

$$\alpha_k = \operatorname{atn}\left(\sum_{i=1}^{n} \cos(k \cdot \theta_i), \sum_{i=1}^{n} \sin(k \cdot \theta_i)\right) \qquad (2)$$

where $\operatorname{atn}(x,y) = \arctan(y/x)$ if $x > 0$ and $\operatorname{atn}(x,y) = \arctan(y/x) + 180°$ if $x < 0$.

If we apply standard procedures (cf. above and Batschelet [1]) to the data set given in figure 1, i.e. perform calculations of the average vector length (r_k) and mean angle (α_k) for $k = 1$ (unimodal) and $k = 2$ (bimodal), we obtain the results shown in figure 2a and b. As seen from this figure, neither of the two descriptions provide a good fit to the observed angular distribution. Furthermore, we fail to detect a statistically significant deviation from random (uniformity) according to the Rayleigh test.

A new technique. The idea behind the new technique is that instead of testing whether an a priori specified clustering of angular directions (e.g. unimodal or bimodal clustering) fits data better than a uniform distribution, we search among a set of possible types of clustering and determine the one that provides the best fit of the data, and subsequently check whether the description obtained deviates significantly from a uniform distribution.

The vector length r_k for different values of k measures the fit of data to different types of modality. As noted previously $k = 1$ pertains to unimodal distributions of angular data while $k = 2$ corresponds to axial data sets. Other integer values of k represent clusters in k angular directions. Similarly, non-integer values of k correspond to intermediate types of clusterings between those of the integer values. For example, $k = 1.5$ corresponds to modes separated by an angle of 240° (360°/1.5).

To obtain the best possible description of a circular data set, r_k has to be maximized. Hence, we will have to find the k-value (k^*) for which r_k attains its maximum (r_{max}). Since a description of data resulting in a large value of k^*, e.g., two well-defined modes separated by angles less than $360°/5 = 72°$ apart, is unlikely to occur in avian orientation data, we have chosen an upper limit of $k = 5$

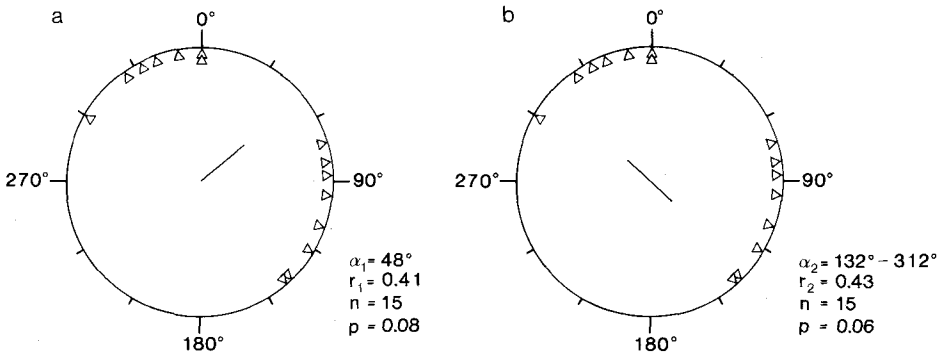

Figure 2. *a* The mean unimodal direction, calculated according to standard procedures given in Batschelet[1], of the data set shown in fig. 1. Mean vector (α_1) of the sample is represented by an arrow whose length (r_1) is drawn relative to the radius of the circle = 1. *b* Average bimodal direction (axis) was calculated by doubling the original angles (θ_i's, cf. table 1) and computing a mean vector angle on the basis of the transformed angles which subsequently was halved. The resulting mean axis (α_2) is illustrated by a double-ended arrow whose length (r_2) is drawn proportional to the radius of the circle = 1. Significance levels (p) are according to the Rayleigh test[1] using r_1 for testing uniformity against unimodality (*a*) and r_2 for testing uniformity against axial bimodality (*b*). Testing uniformity against unimodality and/or bimodality (unspecified), using $r_{1,2} \equiv \max(r_1, r_2) = 0.43$ (cf. text) also yields a non-significant result ($r_{1,2} < 0.49$, cf. table 3). See fig. 1 for further details.

as the basis of meaningful analysis. With other types of circular data, the upper limit of k may be chosen differently, e.g. if it is of interest to detect a distribution where the variance around clusters is small and the modes are situated very close to each other, a higher upper limit of k is appropriate. The practical performance of the technique in such cases is similar to the procedure described here but it should be noted that critical levels as well as detection power depend on the particular interval chosen for investigation.

Under a uniform distribution of angular directions, the average performance of r_k for different k-values may be derived analytically as

$$\sqrt{E(r_k^2)} = \sqrt{\left(\frac{\sin k\pi}{k\pi}\right)^2 + \frac{1}{n}\left(1 - \left(\frac{\sin k\pi}{k\pi}\right)^2\right)}, \quad \text{(where } E$$

stands for expectation), which for large n, i.e. $\lim_{n\to\infty} \sqrt{E(r_k^2)} = \left|\frac{\sin k\pi}{k\pi}\right|$, is given by the dotted line in figure 3. As shown in the figure, the main lobe (broken line) of r_k for k in the interval [0, 1] (corresponding to the hypothetical data set given in fig. 1) is very similar to the expected performance of r_k under uniformity (as described by the dotted line). In practice, k-values below 1 do not permit meaningful analyses and therefore the search for r_{max} will be performed in the interval [1, 5].

How to obtain r_{max}. The search for r_{max} is in practice performed by calculating r_k, as given by equation (1), for a finite set of suitably chosen values of k in the interval [1, 5], e.g. $k = 1.00, 1.05, 1.10, \ldots, 2.00, 2.05, \ldots, 4.95, 5.00$ and then by a direct comparison of the obtained values, selecting the value of k that gives the largest value of r_k. Such a calculation is of course preferably performed by aid of a computer, especially if the number of different values of k is large (a somewhat more crude value may be obtained by using step length = 0.1 which is possible to compute by means of a simple calculator). The largest obtained value constitutes the maximum of r_k for the chosen set of different values of k, while the r_{max} searched for is the maximum in the continuous interval [1, 5]. As a function of k, r_k is continuous, and consequently, r_{max} can be obtained with arbitrary accuracy by decreasing the difference between subsequent k-values. In practice, a value of r_{max} given with sufficient accuracy is usually obtained for k with a step length ranging from 0.1 to 0.01.

Estimation of asymmetric modes. The technique for estimating the modes of a broken axis is summarized in the following steps:

1) Find $k = k^*$ that maximizes r_k (cf. above).
2) Calculate $k^* \cdot \theta_1$, $k^* \cdot \theta_2, \ldots, k^* \cdot \theta_n$, and rearrange the transformed angles in increasing order and denote their values $\phi_1, \phi_2, \ldots, \phi_n$. The k that maximizes r_k is a value such that the transformed angles obtain the best coincidence into a single mode on the circumference of the circle.
3) Calculate α_{k^*} according to equation (2), i.e. $\alpha_{k^*} = \text{atn}\left(\sum_{i=1}^{n} \cos\phi_i, \sum_{i=1}^{n} \sin\phi_i\right)$. The value of α_{k^*} will then show the direction of a particular mode in the interval [0°, 360°] or in some multiple of that same interval, e.g. [360°, 720°].
4) To find the multiple of [0°, 360°] corresponding to the transformed angles of the original two clusters, divide the interval $[\phi_1, \phi_n]$ into two equal parts and calculate the arithmetic mean of the ϕ_i's falling in the first part. Denote this mean ϕ_{m1}. Similarly, calculate the arithmetic mean of the ϕ_i's falling in the second part. Denote this mean ϕ_{m2}.
5) Find n_1 to minimize $|\alpha_{k^*} + n_1 \cdot 360° - \phi_{m1}|$ and n_2 to minimize $|\alpha_{k^*} + n_2 \cdot 360° - \phi_{m2}|$. The mode of the

transformed angles corresponding to the ith cluster is then equal to the n_ith multiple of [0°, 360°], i.e. $n_i = 0$ pertains to [0°, 360°] and $n_i = 1$ corresponds to [360°, 720°] etc.

6) The direction of the first mode angle is given by

$$\alpha_{m1} = (\alpha_{k^*} + n_1 \cdot 360°)/k^*$$

7) The direction of the second mode angle is given by

$$\alpha_{m2} = (\alpha_{k^*} + n_2 \cdot 360°)/k^*$$

We will now exemplify this technique by using the hypothetical data set given in figure 1.

1) As shown in the orientogram (fig. 3), r_k attain its maximum value ($r_{max} = 0.84$) for $k^* = 1.50$.
2) In table 1, the original $\theta_1, \theta_2, \ldots, \theta_n$ is multiplied by $k^* = 1.50$ and the resulting $\phi_1, \phi_2, \ldots, \phi_n$ are arranged in increasing order.

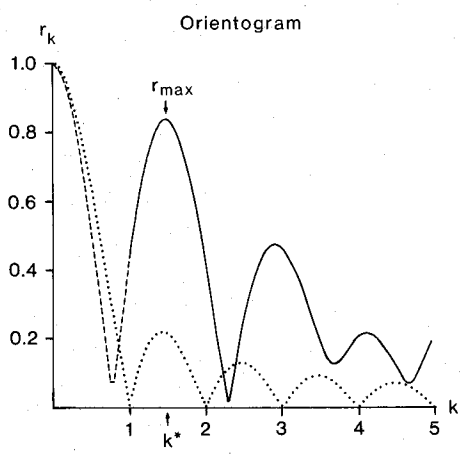

Figure 3. A representation of the relationship between r_k (y-axis) and k (x-axis) called 'orientogram' for the data set in fig. 1 (cf. description of this procedure in the text). As shown in the diagram, r_k attain its maximum value in the interval [1, 5] for $k = 1.50$. For k-values in the interval [0, 1], r_k is illustrated by the broken line. The average performance of r_k for k-values under uniformity, is represented by the dotted line.

Table 1. The original data points (θ_i's) as shown in the hypothetical circular sample in fig. 1. As required by the technique for estimating broken axis (bi-directional and non-antipodal) modes, the basic data points are transformed (to ϕ_i's) by multiplying each of them by $k^* = 1.50$ according to the example given in the text.

Observation	θ_i	$\cdot k^*$	$= \phi_i$
1.	72°	· 1.50	= 112°
2.	82°	· 1.50	= 123°
3.	88°	· 1.50	= 132°
4.	96°	· 1.50	= 144°
5.	110°	· 1.50	= 165°
6.	122°	· 1.50	= 183°
7.	137°	· 1.50	= 206°
8.	140°	· 1.50	= 210°
9.	300°	· 1.50	= 450°
10.	325°	· 1.50	= 488°
11.	333°	· 1.50	= 500°
12.	340°	· 1.50	= 510°
13.	350°	· 1.50	= 525°
14.	359°	· 1.50	= 538°
15.	360°	· 1.50	= 540°

3) Calculation of

$$\alpha_{k^*} = \text{atn}\left(\sum_{i=1}^{n} \cos(k^* \cdot \theta_i), \sum_{i=1}^{n} \sin(k^* \cdot \theta_i)\right)$$

gives $\alpha_{1.50} = 153°$.

4) By dividing the interval [112°, 540°] into two equal parts we get [112°, 326°] and [326°, 540°]. A subsequent calculation of the arithmetic mean of the transformed angles in each of the two intervals yields $\phi_{m1} = 159°$ and $\phi_{m2} = 507°$.
5) Minimization of $|153° + n_1 \cdot 360° - 159°|$ and $|153° + n_2 \cdot 360° - 507°|$ results in $n_1 = 0$ and $n_2 = 1$, respectively.
6) The direction of the first mode angle may now be calculated as $\alpha_{m1} = (153° + 0 \cdot 360°)/1.50 = 102°$.
7) Similarly, the direction of the second mode angle is given by $\alpha_{m2} = (153° + 1 \cdot 360°)/1.50 = 342°$.

The final result of the procedure is shown in figure 4. As became evident in the example, the value of k is not restricted to integers, but any real value of k that maximizes r_k can be used as a starting point when calculating the angular direction of the modes (see above) and the distance between them ($360°/k^*$).

Testing for significance

Concentrating on specific alternatives in a statistical testing procedure improves the power of the test in use when these alternatives are the only interesting ones. Suppose it is desired to test uniformity against the class of alternative densities given by

$$\frac{1}{2\pi}(1 + 2\rho \cos k(\theta - \mu)),\ 0 \leq \theta < 2\pi \qquad (3)$$

for $0 \leq \mu < 2\pi$, $0 \leq \rho \leq 0.5$ and k in some suitable set K of chosen values.

Then a test of uniformity within a class of alternatives can be performed by using a χ^2 statistic, as suggested by Rao [2], by grouping the data into a number of classes with

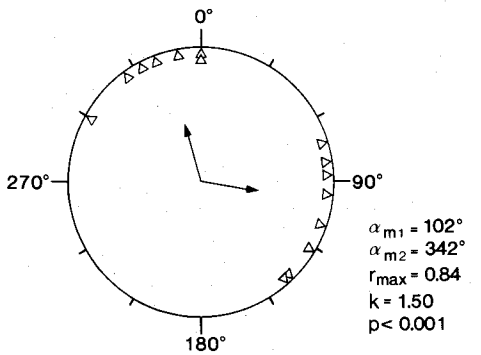

Figure 4. The calculated 'broken-axis' according to the new procedure, developed to estimate non-antipodal modes ($\approx 180°$) of circular distributions (cf. fig. 1). As shown in the figure, the two modes (α_{m1}, α_{m2}) are separated by 120° and the angular distribution is significantly different from random ($p < 0.001$). The maximum value of r_k, corresponding to the least possible orientation scatter as obtained by the 'orientogram analysis' ($k = 1.50$), is indicated by the total length of the broken axis (r_{max}), with arrows pointing towards the two main modes. Significance level is according to table 2.

equal width, followed by a comparison of the estimated cell frequencies under the alternatives with those under the hypothesis.

Testing uniformity within a class of alternatives given by $\frac{1}{2\pi}(1 + 2\rho\cos(\theta - \mu))$ (i.e. $K = \{1\}$) was considered by Rao [3]. He showed that the test statistic in this case is the ordinary Rayleigh statistic, i.e. the length of the resultant vector based on the grouped data. A statistic for non-grouped data can be obtained from the statistic for grouped data by using increasingly finer classifications, which again results in the ordinary Rayleigh statistic that originates from the different angles, i.e. r_1.

Similarly, the test statistic originating from the plausible alternatives given by (3) results in the statistic r_m if k is specified beforehand to be m, i.e. $K = \{m\}$. For $K = \{1,2\}$ the resulting statistic is $r_{1,2} \equiv \max(r_1, r_2)$. The statistic r_{max}, the maximum vector length in a specified interval, is an analogue if k is unspecified within that interval, e.g. given by $K = [1,5]$. In the estimation of asymmetric modes, we utilize the statistic $r_{k^*} = r_{max}$ for testing uniformity against the most predominant clustering type.

The distribution of $2nr_k^2$ (for any integer k) conforms, under uniformity and asymptotically for large sample sizes (n), with the χ^2 distribution with 2 degrees of freedom. This is utilized in the Rayleigh test for rejecting uniformity in preference of unimodality for large values of r_1. Likewise, it is utilized for rejecting uniformity in preference to an alternatively specified cluster in k directions based on the significance level $e^{-nr_k^2}$ for large n. Note that the distribution of $r_{1,2}$ (unimodality or bimodality is unspecified beforehand) conforms under uniformity and asymptotically for large n with the distribution of the maximum of two independent χ^2 variables each with 2 degrees of freedom, i.e. the significance level is $1-(1-e^{-nr_{1,2}^2})^2$ for large n.

Since we search for r_{max} in a larger interval ([1,5]) with finer classifications, the distribution gets more complicated than those of r_1, r_2 and $r_{1,2}$. This is because the probability of finding the maximum of a certain number of variables above a level increases with the number of variables involved, and hence, the probability that the largest value will exceed a certain level is greater than the probability that a preselected variable will exceed that same level. Critical values of r_{max} can be obtained by simulating the distribution of this statistic for a uniform distribution of directions (table 2). The simulation was performed in such a way that n angular directions (fixed sample size) was drawn from a uniform distribution, followed by a calculation of the orientogram r_k for k in the interval [1,5] to obtain r_{max}. This procedure was replicated 10,000 times to obtain the critical values for each sample size and significance level as given in table 2. The critical levels are independent of k, but they do, however, depend on the length of the interval in use (here [1,5]). In table 2, critical values for r_{max} are given for significance levels $p = 0.05$, 0.01 and 0.001.

For comparison, the corresponding critical levels of $r_{1,2}$ i.e., when unimodality or bimodality is unspecified a priori, are shown in table 3.

Table 2. Critical levels of maximum vector length (r_{max}) for k in the interval [1, 5], in relation to sample size, n. If r_{max}, for a given sample size, exceeds the critical level shown in the table, a significant deviation from uniformity is indicated. The critical levels were obtained by computer simulations based on 10,000 replications (see text) for each case of significance level (p) and sample size.

n	$p = 0.05$	0.01	0.001
10	0.72	0.81	0.89
15	0.62	0.70	0.81
20	0.55	0.63	0.70
30	0.47	0.54	0.59
40	0.43	0.48	0.55
50	0.40	0.46	0.52
100	0.34	0.38	0.43

Table 3. Critical levels of maximum of r_1 and r_2 ($r_{1,2}$, cf. text) in relation to sample size, n. If $r_{1,2}$, for a given sample size, exceeds the critical level shown in the table, a significant deviation from uniformity is indicated. The critical levels were obtained by computer simulations based on 10,000 replications for each case of significance level (p) and sample size.

n	$p = 0.05$	0.01	0.001
10	0.59	0.68	0.79
15	0.49	0.58	0.67
20	0.42	0.51	0.59
30	0.35	0.41	0.49
40	0.30	0.36	0.44
50	0.27	0.33	0.39
100	0.19	0.23	0.28

Power of the test

In table 4, the power of detecting deviations from uniformity is compared between the test based on r_{max} and the Rayleigh test, Rao's spacing test and Watson's U_n^2-test, for four different known circular distributions.

Since r_{max} is a test statistic which is sensitive for a large class of alternatives, a loss of power may be expected in comparison to the other statistics for specific distributions such as e.g. r_1 for unimodal distributions and r_2 for axially symmetric distributions. As seen from table 4, r_{max} has large power over the whole range of different distributions, while r_1 and r_2 have large power only for the distributions for which they are constructed to detect (i.e. unimodal and bimodal distributions, respectively). This is also the case for Watson's U_n^2 which is sensitive for unimodal distributions only, and for Rao's spacing test (bimodal case, Rao_2) and Watson's U_n^2 test based on the doubled angles ($U_{n,2}^2$) which have high power for bimodal and quadro-modal distributions only. Rao's spacing test (unimodal case) has high power for all types of the investigated distributions. For small sample sizes the power of Rao's spacing test is of the same order as r_{max}, while for large sample sizes the power of r_{max} is higher.

Table 4. A comparison of the power of maximum vector length (r_{max}) for detecting deviations from uniformity under four known non-uniform circular distributions (when k is in the interval [1, 5]), in relation to other tests; r_1 = Rayleigh test, r_2 = Rayleigh test with doubled angles, Rao = Rao's spacing test, Rao_2 = Rao's spacing test with doubled angles, U_n^2 = Watson's U_n^2 test and $U_{n,2}^2$ = Watson's U_n^2 test with doubled angles, for three different samples sizes. The table gives the probability of rejecting uniformity when data comes from non-uniform unimodal, bimodal, trimodal and quadrimodal distributions, respectively. The power of the different tests was obtained by computer simulations based on 10,000 replications for each case of sample size using the critical value defined on the 5% significance level.

$n = 10$	r_{max}	r_1	r_2	Rao	U_n^2	Rao_2	$U_{n,2}^2$
$\frac{1+\cos\theta}{2\pi}$	0.14	0.54	0.05	0.34	0.52	0.05	0.05
$\frac{1+\cos 2\theta}{2\pi}$	0.32	0.06	0.55	0.30	0.10	0.34	0.53
$\frac{1+\cos 3\theta}{2\pi}$	0.25	0.05	0.05	0.23	0.08	0.05	0.05
$\frac{1+\cos 4\theta}{2\pi}$	0.25	0.05	0.06	0.16	0.06	0.30	0.11
$n = 20$							
$\frac{1+\cos\theta}{2\pi}$	0.44	0.90	0.05	0.56	0.90	0.05	0.05
$\frac{1+\cos 2\theta}{2\pi}$	0.71	0.06	0.90	0.54	0.19	0.55	0.89
$\frac{1+\cos 3\theta}{2\pi}$	0.59	0.05	0.05	0.51	0.10	0.05	0.05
$\frac{1+\cos 4\theta}{2\pi}$	0.57	0.05	0.06	0.47	0.07	0.53	0.19
$n = 30$							
$\frac{1+\cos\theta}{2\pi}$	0.71	0.98	0.05	0.70	0.98	0.05	0.05
$\frac{1+\cos 2\theta}{2\pi}$	0.92	0.06	0.99	0.69	0.35	0.70	0.99
$\frac{1+\cos 3\theta}{2\pi}$	0.83	0.05	0.05	0.69	0.13	0.05	0.05
$\frac{1+\cos 4\theta}{2\pi}$	0.82	0.05	0.06	0.67	0.09	0.69	0.35

Application to a real data set

The ringing recoveries during autumn migration (September and October) of robins *Erithacus rubecula* ringed earlier in the same autumn at Falsterbo Bird Observatory (55° 23'N, 12° 50'E) in southern Sweden is shown in fig. 5A (cf. Sandberg et al. [5]). The angular distribution of the recovery directions is clearly bimodal. However, the two separate modes do not seem to be 180° apart from each other ($r_2 = 0.61$). If we apply the orientogram-technique described above, we find $r_{max} = 0.72$ for $k^* = 2.30$ (fig. 5B). By using this k-value we are able to estimate the corresponding non-antipodal modes that describe the circular distribution of ringing recoveries in a better way ($r_{max} > r_2$). The result generated by this estimation technique (cf. above) is shown in fig. 5C. The two modes are not situated 180° apart, but are separated by a mode-distance of 156° (360°/2.30).

This may provide valuable insights into either the difference between preferred autumn and spring migration directions, or the difference between the seasonally appropriate autumn migration direction and reoriented migration directions.

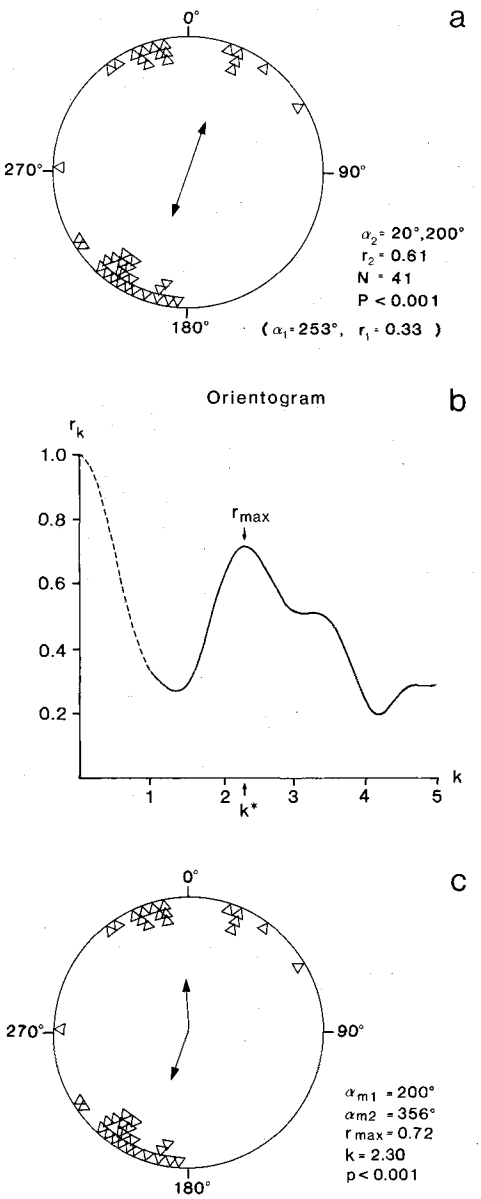

Figure 5. An example of the result obtained when the 'broken axis method' is applied to a real data set. *a* The result of using standard procedures [1] to obtain mean unimodal and bimodal estimates of the circular distribution. The data consist of ringing recoveries of robins captured at Falsterbo Bird Observatory in southernmost Sweden during autumn migration (Sept. and Oct.) and subsequently recovered during the same autumn migration period [5]. As can be clearly seen from the diagram, the mean symmetric bimodal axis does not provide the most satisfactory fit to the observed angular distribution of individual headings. *b* By applying the orientogram procedure, i.e. searching for the k-value that corresponds to the largest r_k we get $r_{max} = 0.72$ for $k = 2.30$, which should be compared to the values of $r_1 = 0.33$ and $r_2 = 0.61$, respectively. *c* Illustration of the final result, after applying the 'estimation of broken axis modes'. As shown in the figure, the resulting description provides a better fit to the observed angular distribution. For further details see fig. 4 and table 2.

Conclusions

The calculations inherent in the new technique are a bit more complicated than standard procedures for obtain-

ing the ordinary unimodal (r_1) and bimodal (r_2) vector lengths to determine whether one-directional or axial clustering fits the data. The calculations are, however, not overwhelming, and compared to the improvement obtained in practical cases where the broken axis approach provides a considerably better fit to the observed data than unimodal and antipodally symmetric bimodal distributions, it seems reasonable to perform the calculations. The method may give a better understanding of the orientation behavior of living organisms, as well as in other areas of research.

A computer program for the calculations inherent in the new technique is available from the authors upon request.

Acknowledgments. We wish to extend our sincere gratitude to Dr Thomas Alerstam for valuable comments and suggestions on earlier drafts of this paper. Furthermore, we thank Steffi Douwes and Kerstin Persson for drawing the figures. The study was financially supported by grants from the Swedish Natural Science Research Council (to B. Holmquist).

1 Batschelet, E., Circular Statistics in Biology. Academic Press, New York 1981.
2 Rao, C. R., Sankhya A *23* (1961) 25.
3 Rao, J. S., Z. Wahrscheinlichkeitstheorie verw. Geb. *22* (1972) 33.
4 Rayleigh, Lord, Phil. Mag. *10* (1880) 73.
5 Sandberg, R., Pettersson, J., and Alerstam, T., Anim. Behav. *36* (1988) 865.

0014-4754/91/080845-07$1.50 + 0.20/0

Vidalols A and B, new anti-inflammatory bromophenols from the Caribbean marine red alga *Vidalia obtusaloba*

D. F. Wiemer*, D. D. Idler and W. Fenical

Scripps Institution of Oceanography, University of California, San Diego, La Jolla (California 92093-0236, USA)
Received 1 November 1990; accepted 20 February 1991

Abstract. Chemical studies of the Caribbean red alga *Vidalia obtusaloba* have resulted in the isolation of two new bromophenolic metabolites, vidalols A and B (**1, 2**). The new compounds were discovered as part of an organized effort to isolate new naturally-occurring anti-inflammatory agents with a focus upon those which may function through the inhibition of phospholipase A_2.
Key words. Anti-inflammatory; bromophenols; red algae; marine natural products.

In connection with our interest in the isolation of new anti-inflammatory compounds from marine sources [1], we have investigated the secondary metabolites of the Caribbean red alga *Vidalia obtusaloba* (Rhodophyta; Rhodomelaceae). Ship-board testing of the crude extract of this alga showed potent in vitro inhibition of bee venom-derived phospholipase A_2 (PLA_2). The subject of this report is the isolation of two new anti-inflammatory bromophenols, vidalols A (**1**) and B (**2**), which inhibit PLA_2 and effectively control edema in the phorbol ester-mouse ear assay [2].

Vidalia obtusaloba (1 kg wet) was collected in shallow water near St. Anne's anchorage, Martinique, in July, 1986. The alga was freeze-dried and repeatedly extracted with 10% methanol in chloroform. After concentration of the combined extracts in vacuo, the crude residue (29 g) was fractionated by silica vacuum flash chromatography. Fractions eluted with 80% EtOAc in isooctane were further purified by gravity elution silica column chromatography to yield vidalol A (**1**, 1.235 g) and vidalol B (**2**, 54 mg) as pure, non-crystalline solids.

Vidalol A (**1**) analyzed for $C_{13}H_9O_5Br_3$ by HRFAB mass spectrometry (M^+ m/z = 481.8029). Fragment ions at m/z 279/281/283 and m/z 216/218 showed that vidalol A was easily cleaved into two benzyl cations with the compositions $C_7H_5O_2Br_2$ and $C_7H_6O_3Br$, respectively. The ^{13}C NMR spectrum of vidalol A in $CDCl_3$ showed 13 resonances, 12 of which were aromatic [3]. A single methylene resonance at 31.9 ppm indicated that vidalol A was a diphenylmethane derivative.

Acetylation of vidalol A with acetic anhydride in pyridine yielded a penta-acetate derivative illustrating that all five oxygen atoms are phenolic hydroxyls. The ^1H NMR spectrum of **1**, recorded in $CDCl_3$ showed two overlapping aromatic protons as broad singlets at δ 6.35 and a broadened 2 H singlet at δ 3.90. These overall data indicated that vidalol A was a diphenylmethane derivative with one ring bearing two bromine atoms and two hydroxyl groups and the other one bromine and three hydroxyl functionalities. The regiochemistry of the substituents on the dibromo-dihydroxy-benzene ring was easily established by comparison of the ^{13}C NMR fea-